DOI: 10.6060/mhc224441b

Magnetocaloric Properties of Lanthanide Tetrapyrrole Complexes above Curie Temperature

Tatyana N. Lomova,[@] Victor V. Korolev, Anna G. Ramazanova, and Olga V. Balmasova

G. A. Krestov Institute of Solution Chemistry of the Russian Academy of Sciences, 153045 Ivanovo, Russian Federation
[@]Corresponding author E-mail: tnl@isc-ras.ru

To obtain the fundamental knowledge in the field of magnetocaloric behavior of new molecular materials at room temperature, we have synthesized (5,10,15,20-tetraphenylporphinato)terbium(III), (5,10,15,20-tetra(4-tert-butylphenyl)porphinato)terbium(III), and (phthalocyaninato)terbium(III) chlorides and have fully characterized their chemical structure using spectral methods (UV-vis, IR, ^{1}H NMR, MALDI TOF). The specific heat capacities of paramagnets synthesized were measured at the temperatures from 223 to 393 K in zero fields using a DSC method. Magnetocaloric effect, heat, and change of enthalpy/entropy during the magnetization were observed over the temperature range of 278 – 328 K in magnetic fields from zero to 1 T by the direct microcalorimetric method. Using the analysis of the temperature dependences of the magnetocaloric parameters in the lanthanide row, we have established that the control of the magnetic exchange between the spin carrier and the paramagnetic ligand is determined both by the fine tuning of the outer shell of the lanthanide ion and by the substitution in the macrocycle. It was shown at a quantitative level that the terbium ion in the tetrapyrrole complexes carries out the magnetic exchange, being in $4f^7 5d^1$ configuration.

Ключевые слова: Magnetocaloric effect, heat capacity, terbium complexes, porphyrins, phthalocyanine.

Магнитокалорические свойства тетрапиррольных комплексов лантанидов выше температуры Кюри

Т. Н. Ломова,[@] В. В. Королев, А. Г. Рамазанова, О. В. Балмасова

Институт химии растворов им. Г.А. Крестова Российской академии наук, 153045 Иваново, Российская Федерация
[@]E-mail: tnl@isc-ras.ru

Для получения фундаментальных знаний в области магнитокалорического поведения новых молекулярных материалов при комнатной температуре нами были синтезированы (5,10,15,20-тетрафенилпорфинато)-тербий(III), (5,10,15,20-тетра(4-трет-бутилфенил)порфинато)тербий(III) и (фталоцианинато)тербий(III) и определена их химическая структура с использованием спектральных методов (ЭСП, ИК, ^{1}Н ЯМР, MALDI TOF). Удельные теплоемкости синтезированных парамагнетиков измеряли при температурах от 223 до 393 К в нулевых полях методом ДСК. Магнитокалорический эффект, выделение тепла и изменение энтальпии/энтропии при намагничивании наблюдали в диапазоне температур 278 – 328 К в магнитных полях от нуля до 1 Тл прямым микрокалориметрическим методом. С помощью анализа температурных зависимостей магнитокалорических параметров в ряду лантанидов установлено, что контроль магнитного обмена между носителем спина и парамагнитным лигандом определяется как тонкой настройкой внешней оболочки иона лантанидов, так и функциональным замещением в макроцикле. На количественном уровне показано, что ион тербия в тетрапиррольных комплексах осуществляет магнитный обмен, находясь в конфигурации $4f^7 5d^1$.

Keywords: Магнитокалорический эффект, теплоемкость, комплексы тербия, порфирин, фталоцианин.

Introduction

A magnetocaloric effect (MCE) *i.e.* the change of the temperature of magnetic material with the change in an external magnetic field is most pronounced at the temperatures near the magnetic phase transition. Lanthanide complexes with porphyrins (H_2Ps) and phthalocyanines (H_2Pcs) act as ferromagnets below the magnetic phase transition temperature. They exhibit magnetism either in the form of packed columnar structures or in the form of single-molecule magnets (SMMs) without the collective magnetic order.[1,2] The development of SMMs with a high relaxation barrier and blocking temperature required for their applications is possible with the deep understanding of the relationships between magnetic properties and the molecular structure. Three parameters are used for increasing the relaxation barrier – the high spin of the carrier ion, splitting in zero ligand field, and exchange between the lanthanide spin carrier and the ligand electronic system. The latter maintains the slow dynamics of magnetization at elevated temperatures and disables fast paths of quantum relaxation. This parameter remains the least studied. The incorporation of paramagnetic metal ions into complexes with electronically excess or radical ligands is one of the most effective ways to achieve a strong magnetic exchange. Zero-dimen-sional SMMs based on tetrapyrrole complexes of lanthanide ions are described in the literature.[3-6] The desirable magnetic characteristics of these complexes namely the effective energy barrier against magnetic relaxation are determined by the ligand field around the lanthanide ion,[3] just as the properties of the strongest magnets as $SmCo_5$ and $Nd_2Fe_{14}B$ are largely a product of fine-tuning the interaction between the lanthanide ion and the crystal lattice.[7] The study of such materials at higher temperatures than Curie one, up to room temperature, where they pass from ferromagnets to paramagnets, is in its infancy.[8,9] However, such studies are associated with the possibility of obtaining information on ways to improve the spin state of a molecule due to ferromagnetic exchange interactions of the central metal ion with paramagnetic ligands through the structural modification of the latter. In particular, this approach is one of the ways to obtain high MCE values in a molecular magnetic material, not necessarily in the vicinity of the magnetic phase transition temperatures.

Along with Dy^{3+}, Tb^{3+} is the first ion from which the researchers focused on the design of molecules with finely tailored ligand fields and large relaxation barriers employing only one or a few highly anisotropic lanthanides were started.[10,11] Latter,[12] these studies have been performed on both the lighter lanthanides exhibiting slow magnetic relaxation under applied fields and the elements of the second half of the lanthanide series which generally possess greater magnetic anisotropy due to a larger unquenched orbital angular momentum.[13] Recently, a new tip of the magnetic interaction between a 4*f* system and a photoexcited macrocycle π system has been found in $TbPc_2^-$, $DyPc_2^-$, a $LnPc_2$ π radical, $TbPc_2^0$, and Ln(TPP)(cyclen).[14-18] The third interaction type in this magneto-optical phenomenon was observed in $LnPc_2$ due to an additional unpaired radical spin.

Our studies of 4*f* metal porphyrins/phthalocyanines promising in electronics/spintronics (room-temperature magnetocaloric materials) are detailed in the works.[19-24] The lanthanide(III) complexes exhibit large MCE at temperatures close to room *e.g.* up to 1.50, 0.455, and 0.38 K in (5,10,15,20-tetraphenylporphinato)- ((AcO)GdTPP), (phthalocyaninato)gadolinium(III) ((AcO)GdPc) acetates, and (5,10,15,20-tetraphenylporphinato)gadolinium(III) acetylacetonate ((Acac)GdTPP), respectively, when the magnetic induction is changed from zero to 1 T. That is only slightly lower than one in 3*d*-4*f* clusters/homo-metallic gadolinium compounds at higher fields (2.4 – 3 K at ΔB of 0 – 7 T).[25] Contributions in MCE value from ferromagnetic and antiferromagnetic interactions between a spin carrier and a macrocycle π system were described using the data of MCE/heat capacity temperature dependences.

The derivatives of Tb^{3+} as the highly anisotropic lanthanide ion were chosen in the present work. We represent here the synthesis of (5,10,15,20-tetraphenylporphinato)terbium(III), (Cl)TbTPP, (5,10,15,20-tetra(4-*tert*-butylphenyl)porphinato)terbium(III), (Cl)TbT^{t}BuPP, and (phthalocyaninato)terbium(III), (Cl)TbPc (Figure 1), chlorides and the description of their magnetocaloric behavior at the temperatures close to room.

The MCE, the heat, and the change of the enthalpy/entropy during the magnetization were for the first time observed over the temperature range of 278 – 328 K and in magnetic fields from zero to 1 T by the direct microcalorimetric method. Specific heat capacity in the solid complexes has been directly determined in the temperature range 223 – 393 K in zero magnetic fields using differential scanning calorimetry. The temperature and field dependences of the magnetization thermodynamic parameters and the heat capacity were used for the estimation of contributions in MCE values. Using the data cited above[19-24] for porphyrin/phthalocyanine complexes of Eu^{3+}, Gd^{3+}, Er^{3+}, Tm^{3+}, Yb^{3+}, we have determined the role of the spin density distribution between the lanthanide ion and equatorial/axial ligands in the formation of the room-temperature magnetocaloric properties of paramagnets based on lanthanide tetrapyrrole complexes employing only one central ion.

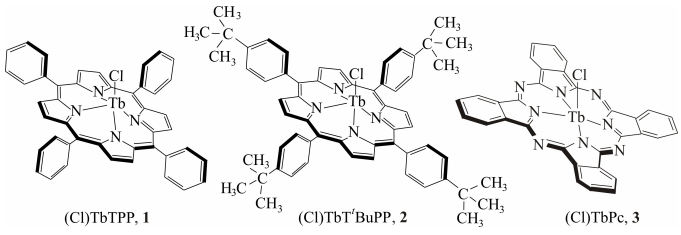

Figure 1. Chemical structure of (5,10,15,20-tetraphenylporphinato)terbium(III) chloride ((Cl)TbTPP), (5,10,15,20-tetra(4-*tert*-butylphenyl)porphinato)terbium(III) chloride ((Cl)TbT^{t}BuPP), and (phthalocyaninato)terbium(III) chloride ((Cl)TbPc).

Experimental

(5,10,15,20-Tetraphenylporphinato)terbium(III) chloride, (Cl)TbTPP (**1**). H_2TPP (0.12 g, 0.19 mmol), 0.11 g (0.29 mmol) of $TbCl_3 \times 6H_2O$ (the minimum excess of salt, at which complexation occurs), and 18 mL of benzonitrile were introduced into a pear-shaped flask with a capacity of 50 mL, equipped with a reflux condenser. The reaction mixture was heated to 215 °C for 9 h. Then the contents of the flask were shaken and hot loaded onto a

column with alumina soaked in chloroform. Chloroform was passed through the column to remove a zone of unreacted H_2TPP. The complex that adsorbed at the top of the column was washed off with a 1% solution of AcOH in ethanol. The complex solution was diluted with an equal volume of chloroform and water was added until the chloroform layer separated. In this case, the complex is completely converted into chloroform. The chloroform part was separated, washed with water from AcOH, and evaporated to dryness to a polycrystalline powder. The (Cl)TbTPP UV-vis spectrum does not change after the second chromatography, *i.e.* a spectrally pure complex is obtained in the process described above. The complex does not change at temperatures up to 250 °C in air and up to 300 °C in a sealed capillary. It is soluble in chloroform, DMF, slightly soluble in alcohol, acetone, and insoluble in water. Yield: 0.08 g (60%). UV-vis (chloroform) λ_{max} (lgε) nm: 591 (3.86), 553 (4.41), 516 (3.82), 422 (5.70), 404 (4.83) (for Figure see Supplementary Data). IR (KBr) ν cm^{-1}: (371, 391), (523, 579), 853 Tb-Cl, 424 νTb-N, 701, 723, 752 γC-H phenyl, 799 γC-H pyrrole rings, 998, 1007, 1033 δC-H pyrrole rings, νC_3-C_4, νC-N, 1070, 1156, 1178, 1201 δC-H phenyl, 1330 νC-N, 1440 νC=N, 1476, νC=C phenyl, 1516 vibrations of the pyrrole rings, 1575, 1596 νC=C phenyl, 3019, 3053 νC-H phenyl. ^{1}H NMR ($CDCl_3$) δ ppm: -85.796 (br.s, $8H_β$), -28.172 (s, $4H_o$), 7.579 (m, $6H_m$), 7.824 and 8.009 (br.s, $2H_p$, br.s, $2H_p$,), 8.386 and 8.632 (br.s, $4H_o$, br.s, $2H_m$). MALDI-TOF (without a matrix) *m/z* (intensity,%): 771.70 (100) $[M - Cl]^+$ (Calculated for $C_{44}H_{28}N_4Tb$ 771.65), 615.67 (76) $[M - Tb – Cl + 2H]^+$ (Calculated for $C_{44}H_{28}N_4$ + 2H 614.74). MALDI-TOF (CHCA) *m/z*: 615.77 $[M – Tb – Cl + 2H]^+$.

5,10,15,20-Tetra(4-tert-butylphenyl)-21H,23H-porphine, H_2^{t}BuPP, was synthesized by the procedure from.[26,27] Pyrrole (3.39 g, 32 mmol) and 4-*tert*-butylbenzaldehyde (5.19 g, 32 mmol) were successively added in drops with constant stirring to 100 mL of boiling propionic acid. After the addition of aldehyde, the reaction mass was refluxed with stirring for 30 min. The solution was cooled to room temperature and placed in a freezer for 12 h. The precipitate formed was filtered off, washed with methanol (3 times with 10 mL) and hot water (3 times with 30 mL). The obtained purple crystals were dried in the air and then in vacuum. Yield: 0.865 g. (12.89%). UV-vis ($CHCl_3$) λ_{max} nm: 649, 590, 554, 518, 421. IR (KBr) ν cm^{-1}: 3313, 2953, 2920, 2851, 1736, 1461, 1262, 1105, 964, 803, 789, 734, 713. ^{1}H NMR (400 MHz, $CDCl_3$) δ ppm: 8.87(s, 8H), 8.155 (d, J = 8.2 Hz, 8H), 7.765 (d, J = 8.2 Hz, 8H), 1.62 (s, 36H), -2.74 (s.br, 2H).

(5,10,15,20-Tetra(4-tert-butylphenyl)porphinato)terbium(III) chloride, (Cl)TbT^{t}BuPP (**2**) was synthesized by the reaction similar to that for (Cl)TbTPP in boiling imidazole. The mixture consisting of 0.02260 g H_2T^{t}BuPP, 0.05264 g of $Tb(Cl)_3×6H_2O$ (the molar ratio is 1:5), and 2.5 g imidazole was heated to 265 °C and boiled under reflux for 1 hour. Then the contents of the flask were cooled, solved in chloroform, washed with hot water from imidazole, and evaporated to dryness. The solid product was dissolved in chloroform and chromatographed using Al_2O_3 as an adsorbent and the solvents, in sequence chloroform, ethanol, and ethanol – 1% AcOH. The solution of complex in ethanol – 1% AcOH obtained at the exit from the chromatographic column was diluted with an equal volume of chloroform and water was added until the chloroform layer separated. In this case, the complex is completely converted into chloroform. The chloroform part was separated, washed with water from AcOH, and evaporated to dryness to a polycrystalline powder. Yield: 25%. UV-vis (chloroform) λ_{max} (lgε) nm: 593 (3.97), 555 (4.34), 517 (3.90), 424 (5.68), 400 (4.52). IR (KBr) ν cm^{-1}: 394, (562, 584), 852 Tb-Cl, 433 νTb-N, 724 γC-H phenyl, 799, 809 γC-H pyrrole rings, 989, 1005, 1026 δC-H pyrrole rings, νC_3-C_4, νC-N, 1067, 1109 δC-H phenyl, 1202, 1267 $–C(CH_3)_3$, 1328 νC-N, 1363, 1394, δC-H $–C(CH_3)_3$, 1462, 1476 νC=N, 1505, 1518, 1577 νC=C phenyl, 2867, 2900, 2962 νC-H $–C(CH_3)_3$, 2987, 3026 νC-H phenyl (Figure S1). ^{1}H NMR (400 MHz, $CDCl_3$) δ ppm: -15.99 (s, $8H_β$), -10.714 (br.s, $4H_o$), 1.377 (s, $36H_{tert\text{-}butyl}$), 7.539, 7.895 (s, $2H_m$, s, $2H_m$), 7.759, 8.287, 8.612 (s, $1H_o$, $1H_o$, $2H_o$). MALDI-TOF (without a matrix) *m/z* (intensity, %): 1184 (6) $[M - Tb – Cl + C_{10}H_7NO_3]^+$, 840.20 (100) $[M - Tb – Cl + 2H]^+$ (Calculated for $C_{60}H_{60}N_4$ +2H 839.17), 418.41 (36) $[M - Tb – Cl + 2H]^{++}$ (Calculated for ½ ($C_{60}H_{60}N_4$ + 2H) 419.59). MALDI-TOF (CHCA) *m/z* (intensity, %): 840.33 (100) $[M - Tb – Cl + 2H]^+$ (Calculated for $C_{60}H_{60}N_4$ +2H 839.17), 418.48 (64) $[M - Tb – Cl + 2H]^{++}$ (Calculated ½ ($C_{60}H_{60}N_4$ +2H) 419.59). MALDI-TOF (DHB) *m/z*: 840.11 $[M - Tb – Cl + 2H]^+$ (Figure S2).

(Phthalocyaninato)terbium(III) chloride, (Cl)TbPc (**3**) was obtained from Li_2Pc and $TbCl_3×6H_2O$ by a method described in.[28] Li_2Pc (0.04943 g) and $TbCl_3×6H_2O$ (0.04680 g) (molar ratio of 1: 3) were introduced into 13 mL of DMSO. The mixture was heated to boiling, kept at boiling temperature for 80 minutes, and cooled. 2 mL of water were added to the reaction mixture. The H_2Pc precipitate was filtered off. The filtrate was diluted 3 times with water. The precipitate of the complex formed after centrifugation was separated by liquid decantation and was dried in air or at the temperature of 373 K. The complex is stable in solid and in solutions in the absence of acids. Yield: about 90%. UV-vis (chloroform) λ_{max} nm: 673, 605, 639 (a shoulder), 341. IR (KBr) ν cm^{-1}: (415, 436), (564, 628), 885 Tb-Cl, 500 νTb-N, 646, 735 γC-H benzene rings, 779 γC-H pyrrole rings, 885, 1005, 1061, 1080, 1162, 1284 δC-H benzene rings, 1168 -C-C- aromatic ring, 1114 isoindole moieties, 1330, 1406 −C=C−N=, 1456 ν isoindole moieties, 1485 −N=, 1559, 1585, 1606 νC=C benzene rings, 3003, 3055 νC-H benzene rings. ^{1}H NMR (400 MHz, $CDCl_3$) δ ppm: -45.5 (br.m, $8H_α$), -17.5 (br.m, $8H_β$). ^{1}H NMR (400 MHz, N,N-dimethylformamide-d_7) δ ppm: -23.0 (br.m, $8H_α$), -8.9 (br.m $8H_β$). MALDI-TOF (without a matrix) *m/z*: 671.55 $[M - Cl]^+$ (Calculated for $C_{32}H_{16}N_8Tb$ 671.46). MALDI-TOF (DHB) *m/z*: 825.85 $[M – Cl + DHB]^+$ (Calculated for $C_{32}H_{16}N_8Tb$ + $C_7H_6O_4$ 825.58). MALDI-TOF (CHCA) *m/z*: 860.98 $[M – Cl + CHCA]^+$ 859.62 (Calculated for $C_{32}H_{16}N_8Tb$ + $C_{10}H_7NO_3$ 859.62).

All reagents were of analytical grade. Chloroform, benzonitrile, propionic acid, DMSO, the phthalocyanine lithium complex and 5,10,15,20-tetraphenyl-21H,23H-porphine, were purchased from Sigma Aldrich.

MCE and magnetization thermodynamics of paramagnets in the polycrystalline form were studied in the temperature range from 278 to 328 K using the microcalorimetric method.[29-31] To do this, the solid samples of terbium(III) complexes were exposed to a magnetic field from zero to 1 Tesla. The solid paramagnet was placed on the bottom of the thermostatically controlled cell with a volume of 2 cm^3, which was then filled with water. The MT-64M brand thermistor and non-induction calibration heater (R = 15.380 Ohm) were allocated in the center of the cell. The cell with the isothermal shell was placed in the gap of the electromagnet (60 mm) made in TIPE JM Japan Electron Optics Laboratory Co., LTD, then the certain temperature was set in the entire system. Temperature changing was registered with the temperature fluctuation of 0.0002 °C. The sensitivity of the setup was 2.10^{-5} ºC. The magnitude of the magnetic field in the electromagnet gap was changed during the experiment from 0 to 1 T. The amount of induction was obtained with an accuracy of 1.5% using a magnetic induction meter Sh-1-8. The current strength of the calibration heater was measured using a reference temperature meter RTM (accuracy class 0.002) connected with a computer. Specially elaborated Delphi language software allowed the online presentation of the change in the resistance of the microthermistor with time and storage of the data to the file for further analysis. The calculation of the MCE value was used by graphical processing of the dependence of temperature change on time and determination of the amount of heat released in the calorimetric experiment because of MCE. The magnetocaloric effect is associated with a change for heat in an isothermal process by the following relation (Eq.1). The reliability of the calorimeter was tested by determining the MCE of metallic gadolinium and is given in.[21]

Heat capacities with an error of about 2% were measured at the temperatures from 223 to 393 K in zero fields using a 204 F1 Phoenix DSC calorimeter (NETZSCH, Germany).

The UV-vis spectra were measured on Agilent 8453 UV-Visible spectrophotometers; IR and ^{1}H NMR spectra were recorded on a VERTEX 80v and Bruker Avance III-500 NMR spectrometers respectively; mass spectrum was performed on Bruker Autoflex.

The temperature change due to the magnetization process (ΔT_{MCE} K), MCE, was calculated with the error not exceed 2% using equation (1). Here $m_{(M)}$ and $C_{p(M)}$ are mass (g) and specific heat capacity (J g^{-1}K^{-1}) of a magnetic material, Q_{MCE} is the amount of heat (J g^{-1}) that was allocated because of MCE in a magnetic material when the magnetic field is switched.

$$\Delta T_{MCE} = Q_{MCE}/m_{(M)}C_{p(M)} \quad (1)$$

For that, the amount of heat, Q_{MCE} (J g^{-1}) was determined (Eq. 2).

$$Q_{MCE} = Q_J (\Delta T/\Delta T_J) \quad (2)$$

Here Q_J – Joule heat (J g^{-1}), injected in the calorimetric experiment, ΔT_J and ΔT – the temperature (K) change of calorimetric system as result of injecting of Joule heat and as a result of a magnetic field change, respectively. Since the MCE values were measured not near the blocking temperature, the specific heat capacity C_p (J g^{-1}K^{-1}) of solid paramagnets in zero fields measured directly in the DSC experiment was taken for the calculation (Eq. 1).

The enthalpy change of a magnetic material, $\Delta H_{(M)}$ J mol^{-1}, resulting from the changes in the magnetic field was determined from the experimental values of Q_{MCE}.

The values of changes in the entropy of paramagnets in the magnetic field, ΔS (J g^{-1}K^{-1}) were calculated by equation (3).[32]

$$\Delta S = - C_{p(M)} \Delta T_{MCE}/T \quad (3)$$

Here, $C_{p(M)}$ is the specific heat capacity, ΔT_{MCE} is the MCE; T is the absolute temperature.

Results and Discussion

The data of the spectral methods, which are represented in Figures 2, 3 and in Supplementary Data, confirm the chemical structure of the Tb complexes in Figure 1. The UV-vis spectra of the porphyrin and phthalocyanine complexes synthesized are represented by the intense band with the maximum Q(0,1) near 550 nm and Q(0,0) near 670 nm, respectively, and low-intensity bands on the right and left for porphyrin complexes and on the left for phthalocyanine complex. There is the complex Soret band near 420 nm and 340 nm, respectively, in the shortwave part of the spectrum. The low-intensity bands at 591–593 nm and 516–517 nm in the terbium porphyrin spectra are Q(0,0) and Q(0,2), respectively, while the low-intensity band with the maximum at 605 nm in the (Cl)TbPc spectrum is the absorption Q(0,0) band vibrational satellite. [33-35] The UV-vis spectrum tests has showed the stability of (Cl)TbPc, (Cl)TbTPP, and (Cl)Tb^{t}BuPP in the microcalorimetric and DSC experiments (Table S1). The macrocyclic and coordinated nature of the compounds synthesized manifests itself in the displaying of the signals that are related to the macrocycle bonds/fragments and the Tb-N/Tb-Cl bonds in the IR spectra (Supplementary Data, Figure S4). Broadened and shifted signals in the ^{1}H NMR spectra of the Tb complexes compared with these in the spectra of uncoordinated H_2Ps and diamagnetic MPs/MPcs[8] point to the paramagnetic character of the compounds studied. The upfield shift of the macrocyclic proton signals compared to diamagnetic complexes of porphyrins/phthalocyanines due to the presence of the paramagnetic terbium ion is observed for all three complexes synthesized. However, its value sharply depends on the structure of the complex, decreasing from (Cl)TbTPP (β protons) to (Cl)TbPc (α and β protons) and further to (Cl)Tb^{t}BuPP (β protons). The weak signal at –3.0 ppm (m, 0.2H) in the (Cl)Tb^{t}BuPP spectrum (Figure S2) related, probable, to the porphyrin free base in trace amounts, which, however, does not form a separate zone on the thin layer chromatogram and does not affect (Cl)Tb^{t}BuPP magnetocaloric behavior due to diamagnetic nature.

MALDI TOF mass spectra of the Tb complexes studied is very specific. The M-Cl bond dissociation during mass spectrum registration is a well-known fact not only for lanthanide tetrapyrrole complexes, but for the complexes of *d* metal ions.[36] A molecular ions of terbium complexes studied, $[M\text{-}Cl]^+$, are observed if a mass spectrum is performed without any matrix (Figure 3), while the use of DHB or CHCA as a matrix has resulted in the substitution of the axial Cl^- ligand by the matrix molecule or in dissociation of a coordination center (Figure S5, S6). A matrix molecule can even occur from residual impurities in the device. The Supplementary Data shows that dissociation of a coordination center is observed for (Cl)TbTPP and (Cl)Tb^{t}BuPP, the stability of which is significantly lower than the one of the Tb phthalocyanine complex[8,37] and, especially, of the complexes with *d* metal ions.[38,39] The reaction rate constant in ethanol – 0.14 M AcOH, k^{298K}, is $0.14\cdot10^{-5}$ s^{-1} and $3.4\cdot10^{-4}$ s^{-1} for (AcO)TbPc and (AcO)TbTPP, respectively. The coordination center in isostructural complexes of *d* metal ions is unstable only in highly acidic solvents as AcOH – H_2SO_4 mixtures.

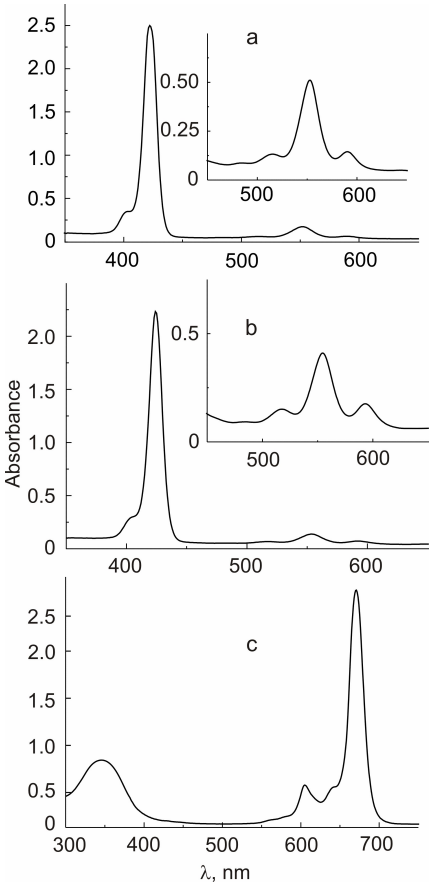

Figure 2. The UV-vis spectra of (Cl)TbTPP (a), (Cl)Tb^{t}BuPP (b), and (Cl)TbPc (c) in chloroform.

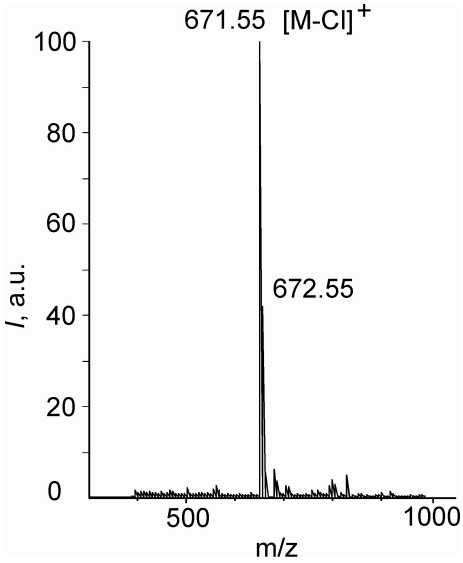

Figure 3. The MALDI TOF mass spectrum of (phthalocyaninato)-terbium(III) chloride (M = 706.9104 g mol^{-1}) without a matrix.

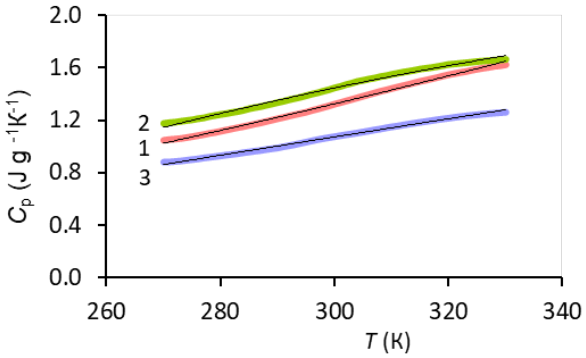

Figure 4. The temperature dependence of the specific heat capacity of (Cl)TbTPP (1), (Cl)TbT^{t}BuPP (2), and (Cl)TbPc (3) in zero magnetic fields.

The experimental specific heat capacities obtained at temperatures from 223 to 393 K together with the calculated molar heat capacities are listed in Tables S2 – S4 and shown in Figure 4.

The specific heat capacities for the corresponding sequence of terbium complexes are fitted to the polynomials (Eq. 4 - 6) for the qualitative interpretation of contributions in the MCE value.

$$C_p\,(\text{J g}^{-1}\text{K}^{-1}) = 1\cdot10^{-5}x^2 + 0.0026\,x - 0.6246 \quad (4)$$

The correlation coefficient of the fitting $R^2 = 0.99$.

$$C_p\,(\text{J g}^{-1}\text{K}^{-1}) = -3\cdot10^{-5}\,x^2 + 0.0276\,x - 4.0538 \quad (5)$$

The correlation coefficient of the fitting $R^2 = 0.99$.

$$C_p\,(\text{J g}^{-1}\text{K}^{-1}) = -2\cdot10^{-6}\,x^2 + 0.0081x - 1.184 \quad (6)$$

The correlation coefficient of the fitting $R^2 = 0.99$.

The heat capacity values slowly increase with increasing temperature. The fact that the (Cl)TbT^{t}BuPP specific heat capacity values are higher than these of (Cl)TbTPP and (Cl)TbPc seen from the represented data demonstrates the more loose structure of the Tb complex substituted with the bulky *tert*-buthyl groups. No pronounced maxima are observed, which points to no phase transition in the temperature range taken.[40]

Determination of numerical values of magnetic material heat capacity and thermodynamic parameters of its magnetization is itself an important task of magnetochemistry. Besides the analysis of the temperature dependencies of these characteristics gives the possibilities namely provides to estimate qualitative the contributions to the magnetic behavior of the studied samples. Therefore, the temperature dependences of the magnetocaloric parameters for the paramagnetic Tb complexes are under discussion in our work.

The field and temperature dependences of room-temperature MCE in (Cl)TbT^{t}BuPP, (Cl)TbTPP, and (Cl)TbPc are shown in Figures 5, 6, S7, and S8.

Being inversely proportional to the specific heat capacity (Eq. 1), MCE decreases when the C_p values increase with the temperature growth reaching the plateau at temperatures above 300 K. This is not where the reverse similarity of the two dependencies ends. The dependence lines of two porphyrin complexes almost converge at the temperature of 328 K. The same can be below seen on the dependence graphs of the entropy change under magnetization *vs* temperature. That can mean the significant contribution in MCE from the paramagnet lattice subsystem, which dominates over the contribution of the electronic subsystem. However, despite the higher C_p values, (Cl)TbT^{t}BuPP demonstrates the highest MCE, while the opposite is true for the phthalocyanine derivative, (Cl)TbPc (Figures 4, 6).

That indicates the appreciable contribution in MCE from the lattice subsystem as well from the electronic subsystem, which in sum determines the magnetic behavior of the Tb complexes studied.

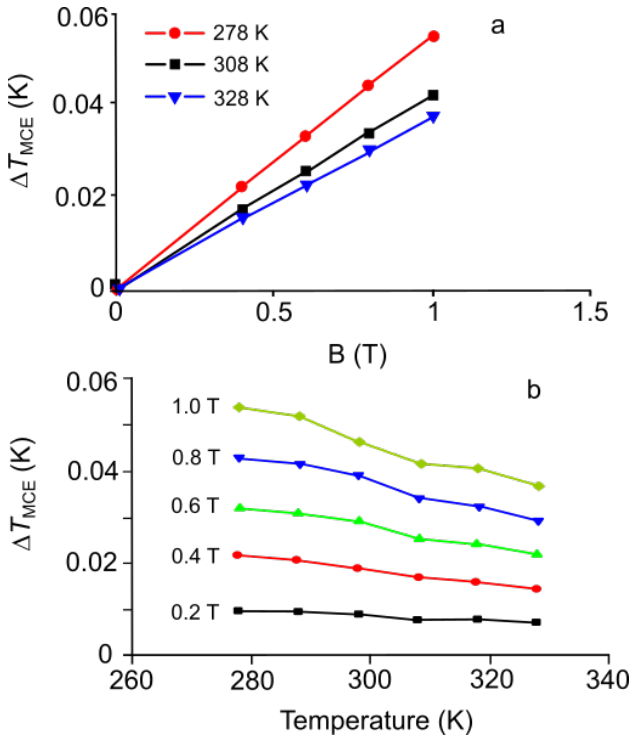

Figure 5. Magnitudes of magnetocaloric effects in (Cl)TbT^{t}BuPP as functions of magnetic induction (a) and temperature (b).

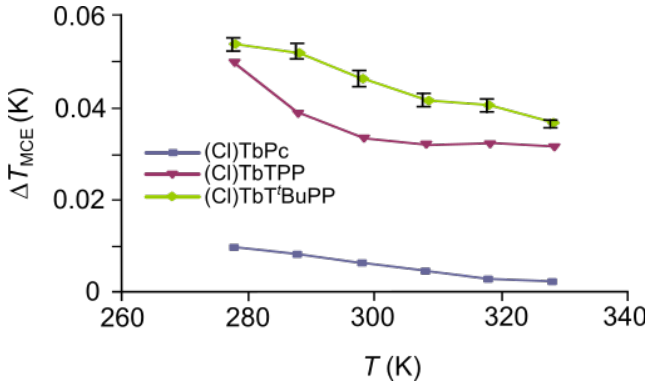

Figure 6. The temperature dependences of MCE in (Cl)TbT^{t}BuPP, (Cl)TbTPP, and (Cl)TbPc at the magnetic induction 1.0 T.

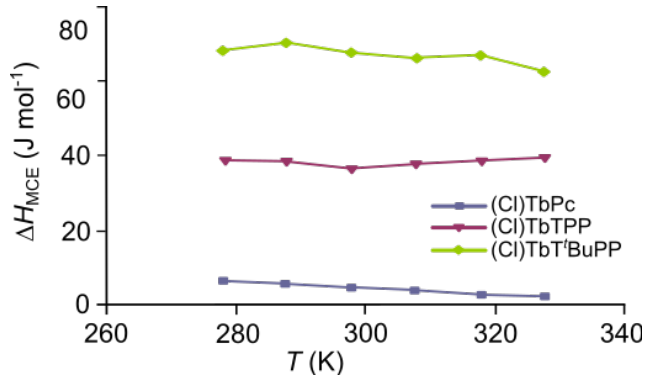

Figure 7. The temperature dependences of the enthalpy change due to the magnetization of (Cl)TbT^{t}BuPP, (Cl)TbTPP, and (Cl)TbPc at the magnetic induction 1.0 T.

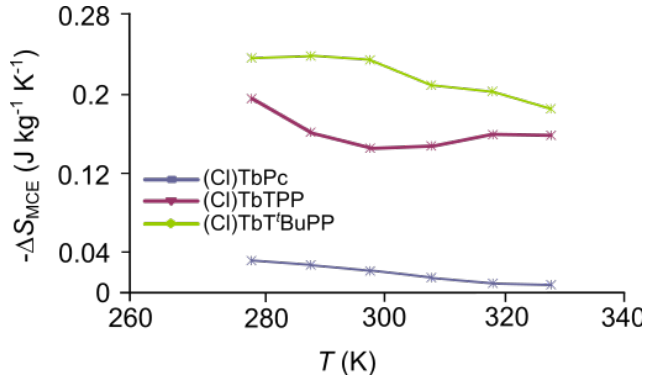

Figure 8. The temperature dependences of the change in the entropy of Tb complexes at the magnetic induction 1.0 T.

The temperature dependences of the calculated enthalpy changes of the magnetization, ΔH J mol^{-1}, at various magnetic fields are shown in Figures 7, S9 – S11.

The experimental values of the specific heat, Q_{MCE} (J g^{-1}), allocated in the Tb complexes because of MCE, which are the direct parameters for estimating the cooling capacity, are represented in Figures S12 – S14 depending on temperature and magnetic field. The above two contributions to the MCE result in temperature dependences of ΔH that do not follow the MCE curves.

The values of the change in the entropy of Tb complexes in magnetic field, ΔS (J g^{-1}K^{-1}), (Figures 8, S15 – S17) were calculated on the assumption of the far location of the studied temperature range from the paramagnet phase transition temperatures. The Maxwell's relations and the equation of the total differential of the total entropy of the magnetic system[41] applicable in relatively weak magnetic fields were used.[42]

As expected, the character of the temperature dependencies of ΔS is in good agreement with to that for ΔT_{MCE} and C_p. The (Cl)TbTPP entropy change decreases with the temperature increase in the low-temperature curve section where C_p increases most noticeably for this complex (Figure 4).

The positive MCE values increase with an increase in the magnetic induction and usually decrease with temperature rise (Figures 5, 6). The MCE values of the Tb complexes are two orders of magnitude lower than for the polycrystalline Gd as standard[43] but are comparable to these for the tetrapyrrole complexes of some other lanthanide ions (see in Figure 9).

To determine the nature of the electronic subsystem contribution in MCE should refer to data on the stability of the Tb complexes and their $\pi \rightarrow \pi^*$ transition energies (the wavelength of the maximum of the first absorbance band in the UV-vis spectrum). These energies correlate with the zero-field energy gap between the two lowest levels equal to the effective barrier against the magnetic relaxation in SMMs based on lanthanide phthalocyanines.[3]

There are the constants of the (Cl)TbTPP/(Cl)TbPc kinetic stability in the literature.[8,44-46] The sharp increase of the kinetic stability of lanthanide phthalocyanines at the beginning of the yttrium sub-group from Gd to Tb evidences the participation of $4f^8$ electrons in the form of $4f^7 5d^1$ in the dative π-bonding Ln→N in the Tb complex. This could be connected with the striving of the Tb atom in the complex for the stable f^7 configuration and with the presence of the vacant π-orbitals of low energy in the macrocycle.

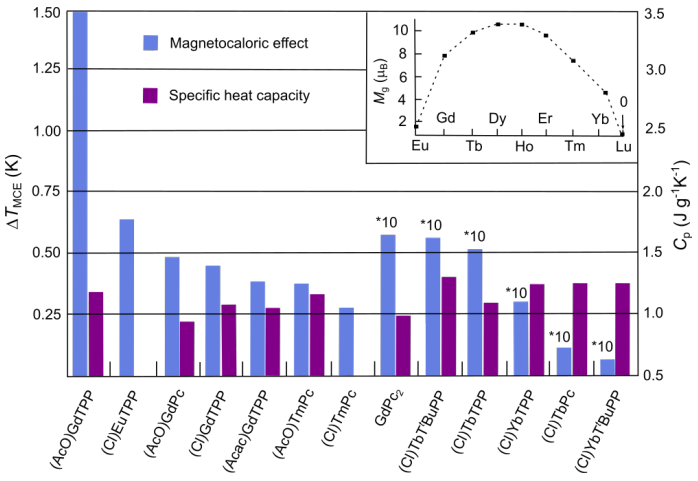

Figure 9. The MCE (278 K, 1 T) sensitivity graph of polycrystalline lanthanide complexes with aromatic tetrapyrroles to modifications in the axial/equatorial ligand and central atom (insert: the dependence of the Ln^{3+} magnetic moments on the serial number of lanthanide at the temperature of 300 K created using the data of work[47]).

The transition of the eighth 4*f*-electron to the 5*d* orbital increases the Tb ion spin while the dative Ln→N bonding leads to the deterioration of the spin state of the spin carrier. The same pattern was found in the case of the porphyrin complex. Wherein the increase in the kinetic stability from (Cl)TbTPP to (Cl)TbPc characterized by the observed dissociation rate constant of $101 \cdot 10^{-4}$ s^{-1} and $0.23 \cdot 10^{-4}$ s^{-1} in the ethanol–0.71 M AcOH and ethanol–2.13 M AcOH medium, respectively, corresponds the decrease in MCE (Figure 6). In this way, the redistribution of the Tb spin density due to the macrocycle participation is a negative contribution in MCE and worsens the magnetocaloric properties of Tb complexes with both porphyrin and phthalocyanine. The relative position of the maximum of the first absorbance bands in the (Cl)TbTPP and (Cl)TbPc UV-vis spectra at 591 nm and 675.2 nm, respectively,[8] does not contradict the above conclusion about the electronic subsystem contribution in the MCE values. Characteristically, the positive electronic effect of the four *tert*-butyl substituents located in the para-position of the phenyl reduces the probability of the dative interaction Ln→N, which should make a positive contribution to the value of the MCE (Cl)TbT^{t}BuPP. Exactly this effect is observed in practice (Figure 6). As will be seen from the diagram below (Figure 9), the effect of *tert*-butyl substitution in the MCE value can be the opposite. The Yb←N π dative bond in (Cl)YbTPP is always directed from the macrocycle to central atom acting to decrease the MCE value due to the specific electron f^{13} configuration with the single unpaired electron. As the result, the (Cl)YbT^{t}BuPP MCE value is lower than the one in (Cl)YbTPP (0.054 K and 0.051 K, respectively, at 278 K and the magnetic induction change from 0 to 1 T).[24]

Figure 9 created using the data of this work and earlier published results[21-24,48] represents the MCE and C_p values for the studied paramagnets based on porphyrin/phthalocyanine lanthanide complexes, which are shown in the decreasing order of the MCE magnitude. It is seen that no correlations between the MCE values and both the heat capacity values and the magnetic moments of the lanthanide ions are observed. That means the basic contribution in the magnetocaloric behavior of the paramagnets under discussion from the exchange interactions between a ligand aromatic system and a central lanthanide ion as well as from the spin state of a latter.

The best samples of the lanthanide complexes exhibit a large MCE at temperatures close to room e.g. up to 1.45 K, 0.623 K, and 0.455 K in (AcO)GdTPP, (Cl)EuTPP and (AcO)GdPc, respectively, when the magnetic induction is changed from zero to 1 T (Figure 9). These values are only slightly lower than the ones in 3*d*-4*f* clusters/homo-metallic gadolinium compounds at higher fields (2.4–3 K at ΔB of 0–7 T)[25] and significant higher compared to the rare-earth-free systems as $Al_xCr_{0.25}MnFeCo_{0.25-y}Ni_y$ (x = 0–0.5, y = 0–0.25) alloys.[49]

Contributions in a MCE value of (porphyrinato)/(phthalocyaninato) lanthanide(III) complexes include a positive and a negative part. Increasing ligand-field splitting and a high spin state of a central lanthanide ion in a porphyrin/phthalocyanine complex is always a positive contribution in MCE. Spin density delocalization with the participation of a macrocycle π electron system, namely π dative interaction M-N effects on a MCE value depending on the electron configuration of a lanthanide ion with an asymmetrically filled *f*-shell. The mentioned double effect from the striving of the Tb atom in the tetrapyrrole complexes for the stable configuration of 4*f* shell, expressed in the dative Tb→N bonding, will always manifest itself as the negative contribution in the spin state of similar Yb complexes exhibiting a reduced MCE (Figure 9). The N→Eu (f^6) and N←Tm (f^{12}) π bonding in (Cl)EuTPP and (Cl)TmPc, respectively, are responsible for appearing and improving of their spin state. It is no coincidence that the porphyrin/phthalocyanine complexes with Eu^{3+} and Tm^{3+} demonstrate the MCE (Figure 9) commensurate with that for the Gd complexes formed by the lanthanide ion with both the stable electron configuration f^7 and the highest spin.

Negative contribution in lanthanide porphyrin/phthalocyanine MCE is obtained from increasing of a mass and a specific heat capacity (Eq. 4), spin carrier interactions with nuclear spins (increasing of macrocycle bonding), and depending on electron configuration from π dative interaction between a central metal ion and a macrocyclic ligand (the N→Tm (f^{12}) π bonding in (Cl)TmPc). An important role in the formation of a porphyrin/phthalocyanine-based paramagnet spin state belongs to antiferromagnetic coupling if the one is possible. MCE of 0.47 K in (AcO)GdPc at 278 K when the magnetic field is changed from zero to 1 T decreases almost an order of magnitude by the transition to the sandwich analog, $GdPc_2^{\bullet}$ (Figure 9[21]), in which one of two macrocycles has been oxidized. The intramolecular oxidation-activated spin coupling does not prevail over the intermolecular coupling of two radical spins of the two neighboring molecules. Additionally, there is electronic interaction that couples the 4*f* electronic system with magnetic momentum **J** and a photo-excited cyclic π-conjugated system with an orbital angular momentum **L** (magneto-optical phenomena caused by the "**J**-**L** interaction") in the Tb/Dy phthalocyanine double-decker complexes.[14,15]

Conclusions

Porphyrin/phthalocyanine complexes with paramagnetic lanthanide ions are of particular interest as molecular paramagnets at temperatures above the Curie temperature. The highest room-temperature MCE values of the paramagnetic lanthanide porphyrin/phthalocyanine complexes are comparable to those for 3*d*-4*f* clusters/homo-metallic gadolinium compounds. That, together with safe for the environment, lower cost compared to expensive metallic gadolinium, solubility in organic media, solution-processability, and the possibility of control of magnetocaloric properties through modifications in a molecule structure, need to take into account when creating new magnetic refrigerators, medical hyperthermia preparations, and magnetic soft robots. Scientific interest in paramagnets of this class is in obtaining information about contributions in their magnetocaloric behavior namely in their spin state formation.

Using the comparative analysis of the temperature dependences of heat capacity and magnetization thermodynamic parameters namely MCE, heat, and an enthalpy/entropy change for terbium complexes studied and for described earlier complexes of other lanthanides, a

positive contribution in MCE was revealed. This contribution is represented by the increase in ligand-field splitting, by a high spin state of a central lanthanide ion in a porphyrin/phthalocyanine complex, and by ferromagnetic exchange interactions between a spin carrier and a variable aromatic macrocyclic system. Negative contribution in lanthanide porphyrin/phthalocyanine MCE is obtained from increasing of a mass and a specific heat capacity, spin carrier interactions with nuclear spins (increasing of macrocycle bonding), and antiferromagnetic exchange interactions between a spin carrier and an aromatic system of a macrocycle. The formation of positive or negative contribution in a MCE value from exchange interactions is only determined by the properties of a lanthanide 4*f* shell while its magnitude depends from both the structure of a tetrapyrrole ligand and the electronic nature of substituents in it.

Acknowledgements. The work was performed within the State task for 2022 - 2024, Topic 122040500043-7, Topic 122040500044-4 and supported by the Russian Foundation for Basic Research (18-43-370022-r-a). That was carried out with the help of the center of the scientific equipment collective use «The upper Volga region center of physic-chemical research». The authors are grateful to the researcher E. G. Mozhzhukhina and Dr. E. N. Ovchenkova for participating in the experiments.

References

1. Giménez-Agulló N., de Pipaón C.S., Adriaenssens L., Filibian M., Martínez-Belmonte M., Escudero-Adán E.C., Carretta P., Ballester P., Galán-Mascarós J.R. *Chem. Eur. J.* **2014**, *20*, 12817–12825. DOI: 10.1002/chem.201402869.
2. Wang H., Wang B.-W., Bian Y. Gao S.J. *J. Coord. Chem. Rev.* **2016**, *306*, 195–216. DOI: 10.1016/j.ccr.2015.07.004.
3. Magnani N. *Int. J. Quant. Chem*. **2014**, *114*, 755–759. DOI: 10.1002/qua.24656.
4. Fukuda T., Shigeyoshi N., Yamamura T., Ishikawa N. *Inorg. Chem*. **2014**, *53*, 9080–9086. DOI: 10.1021/ ic501028f.
5. Ishikawa N., Sugita M., Wernsdorfer W. *Angew. Chem. Int. Ed*. **2005**, *44*, 2931–2935. DOI: 10.1002/anie.200462638.
6. Zhang P., Guo Y.-N., Tang J. *Coord. Chem. Rev*. **2013**, *257*, 1728–1763. DOI: 10.1016/j.ccr.2013.01.012.
7. Rinehart J.D., Long J.R. *Chem. Sci*. **2011**, *2*, 2078–2085. DOI: 10.1039/C1SC00513H.
8. Lomova T.N. *Axially Coordinated Metalloporphyrins in Science and Practice*. Moscow: Krasand, **2019**, 704 p. [Ломова Т.Н. *Аксиально координированные металлопорфирины в науке и практике*, М.: Красанд, 2019. 704 с.], *https://www.rfbr.ru/rffi/ru/books/o 2087172*.
9. Koifman O.I., Ageeva T.A., Beletskaya I.P., Averin A.D., Yakushev A.A., Tomilova L.G., Dubinina T.V., Tsivadze A.Yu., Gorbunova Yu.G., Martynov A.G., Konarev D.V., Khasanov S.S., Lyubovskaya R.N., Lomova T.N., Korolev V.V., Zenkevich E.I., Blaudeck T., von Borczyskowski Ch., Zahn D.R.T., Mironov A.F., Bragina N.A., Ezhov A.V., Zhdanova K.A., Stuzhin P.A., Pakhomov G.L., Rusakova N.V., Semenishyn N.N., Smola S.S., Parfenyuk V.I., Vashurin A.S., Makarov S.V., Dereven'kov I.A., Mamardashvili N.Zh., Kurtikyan T.S., Martirosyan G.G., Burmistrov V.A., Aleksandriiskii V.V., Novikov I.V., Pritmov D.A., Grin M.A., Suvorov N.V., Tsigankov A.A., Fedorov A.Yu., Kuzmina N.S., Nyuchev A.V., Otvagin V.F., Kustov A.V., Belykh D.V., Berezin D.B., Solovieva A.B., Timashev P.S., Milaeva E.R., Gracheva Yu.A., Dodokhova M.A., Safronenko A.V., Shpakovsky D.B., Syrbu S.A., Gubarev Yu.A., Kiselev A.N., Koifman M.O., Lebedeva N.Sh., Yurina E.S. *Macroheterocycles* **2020**, *13*, 311–467, DOI: 10.6060/ mhc200814k.
10. Ishikawa N., Sugita M., Ishikawa T., Koshihara S.-Y., Kaizu Y. *J. Am. Chem. Soc*. **2003**, *125*, 8694–8695. DOI: 10.1021/ ja029629n.
11. Ishikawa N., Sugita M., Okubo T., Tanaka N., Iino T., Kaizu Y. *Inorg. Chem*. **2003**, *42*, 2440–2446. DOI: 10.1021/ ic026295u.
12. Demir S., Meihaus K.R., Long J.R. *J. Organomet. Chem*. **2018**, *857*, 164–169. DOI: 10.1016/j.jorganchem.2017.10.035
13. Ishikawa N., Sugita M., Ishikawa T., Koshihara S., Kaizu Y. *J. Phys. Chem. B*. **2004**, *108*, 11265–11271. DOI: 10.1021/ jp0376065.
14. Kizaki K., Ozawa H., Kobayashi T., Matsuoka R., Sakaguchi Y., Fuyuhiro A., Fukuda T., Ishikawa N. *Chem. Comm*. **2017**, *53*, 6168–6171. DOI: 10.1039/C7CC02960H.
15. Fukuda T., Ozawa H., Sakaguchi Y., Kizaki K., Kobayashi T., Fuyuhiro A., Ishikawa N. *Chem. Eur. J*. **2017**, *23*, 16357–16363. DOI: 10.1002/chem.201703588.
16. Sakaguchi Y., Kizaki K., Fuyuhiro A., Fukuda T., Ishikawa N. *Inorg. Chem.* **2018**, *57*, 15438–15444. DOI: 10.1021/ acs.inorgchem.8b02743.
17. Santria A., Fuyuhiro A., Fukuda T., Ishikawa N. *Inorg. Chem*. **2017**, *56*, 10625–10632. DOI: 10.1021/acs.inorgchem. 7b01546.
18. Santria A., Ishikawa N. *Inorg. Chem*. **2020**, *59*, 14326–14336. DOI: 10.1021/acs.inorgchem.0c02107.
19. Korolev V.V., Lomova T.N., Korolev D.V., Ramazanova A.G., Mozhzhuhkina E.G., Ovchenkova E.N. In: *Environmental Analysis: Applicationals of Nanomatireals* (Hussain C.M., Kharisov B., Eds.) Cambridge: Advanced Royal Society of Chemistry **2016**, p. 14–47.
20. Lomova T.N., Korolev V.V., Zakharov A.G. *Mat. Sci. Eng. B* **2014**, *186*, 54–63. DOI: 10.1016/j.mseb.2014.03.006
21. Korolev V.V., Lomova T.N., Ramazanova A.G., Korolev D.V., Mozhzhuhkina E.G. *J. Organomet. Chem*. **2016**, *819*, 209–215. DOI: 10.1016/j.jorganchem.2016.07.002.
22. Korolev V.V., Lomova T.N., Ramazanova A.G., Mozhzhuhkina E.G. *Mend. Comm*. **2016**, *26*, 301–303. DOI: 10.1016/j.mencom.2016.07.011
23. Korolev V.V., Lomova T.N., Mozhzhuhkina E.G. *Synt. Met*. **2016**, *220*, 502–507. DOI: 10.1016/j.synthmet.2016.07.026.
24. Korolev V.V., Lomova T.N., Ramazanova A.G., Balmasova O.V., Mozhzhuhkina E.G. *J. Porphyrins Phthalocyanines* **2019**, *23*, 1110–1117. DOI: 10.1142/S1088424619501220.
25. Sharples J.W., Collison D. *Polyhedron* **2013**, *66*, 15–27. DOI: 10.1016/j.poly.2013.08.005.
26. Adler A.D., Longo F.R., Finarelli J.D., Goldmacher J., Assour J., Korsakoff L. *J. Org. Chem.* **1967**, *32*, 476. DOI: 10.1021/jo01288a053.
27. Bichan N.G., Ovchenkova E.N., Gruzdev M.S., Lomova T.N. *J. Struct. Chem.* **2018**, *59*, 711–719. DOI: 10.1134/ S0022476618030320.
28. Lomova T.N. Russ. *J. Inorgan. Chem*. **2015**, *60*, 1123–1128. DOI: 10.1134/S0036023615090119.
29. Korolev V.V., Korolev D.V., Ramazanova A.G. *J. Therm. Anal. Calorim*. **2018**, *136*, 937–941. DOI: 10.1007/s10973-018-7704-y.
30. Korolev V.V., Romanov A.S., Arefyev I.M. *Russ. J. Phys. Chem. A*. **2006**, *80*, 464–466. DOI: 10.1134/S003602440 6030277.
31. Korolev V.V., Klyueva M.E., Arefyev I.M., Ramazanova A.G., Lomova T.N., Zakharov A.G. *Macroheterocycles* **2008**, *1*, 68–71. DOI: 10.6060/mhc2008.1.68.
32. Pecharsky V.K., Gschneidner Jr. K.A., Pecharsky A.O., Tishin A.M. *Phys. Rev. B* **2001**, *64*, 144406. DOI: 10.1103/ PhysRevB.64.144406.
33. Subbotin N.B., Tomilova L.G., Kostromina N.A., Lukyanets E.A. *Zh. Obshch. Khim.* **1986**, *5,* 397–400.

34. Gouterman M., Hanson L.R., Khalil G.–E., Buchler J.W., Rohbock K., Dophin D. *J. Am. Chem. Soc.* **1975**, *97*, 142–149. DOI: 10.1021/ja00844a037.
35. Pushkarev V.E., Tomilova L.G, Nemykin V.N. *Coord. Chem. Rev.* **2016**, *319*, 110–179. DOI: 10.1016/j.ccr.2016.04.005.
36. Korolev V.V., Lomova T.N., Ramazanova A.G., Balmasova O.V., Mozhzhukhina E.G. Synth. Met. 2021, *274*, 116696–116702. DOI: 10.1016/j.synthmet.2021.116696.
37. Lomova T.N., Klyueva M.E., Koifman O.I. *Macroheterocycles* **2015**, *8*, 32–46. DOI: 10.6060/mhc140599l.
38. Lomova T.N., Volkova N.I., Berezin B.D. *Zh. Neorg. Khim.* **1987**, *32*, 969–974.
39. Lomova T.N., Berezin B.D., Oparin L.V., Zvezdina V.V. *Zh. Neorg. Khim.* **1982**, *27*, 683–688.
40. Gurek A.G., Basova T., Luneau D., Lebrun C., Kol'tsov E., Hassan A.K., Ahsen V. *Inorg. Chem*. **2006**, *45*, 1667–1676. DOI: 10.1021/ic051754n.
41. Kittel C. *Elementary Statistical Physics*. New York: Wiley, **1958**.
42. Pecharsky V.K., Gschneidner Jr K.A., Pecharsky A.O., Tishin A.M. *Phys. Rev. B* **2001**, *64*, 144406. DOI: 10.1103/ PhysRevB.64.144406.
43. Andreenko A.S., Belov K.P., Nikitin S.A., Tishin A.M. *Physics-Uspekhi (Advances in Physical Sciences)* **1989**, *158*, 553–579. DOI: 10.3367/UFNr.0158.198908a.0553.
44. Lomova T.N., Andrianova L.G., Berezin B.D. *Zh. Fiz. Khim*. **1987**, *61*, 2921–2928.
45. Lomova T.N., Klyueva M.E. Double and Triple Decker Phthalocyanines/Porphyrins. In: *Encyclopedia of Nanoscience and Nanotechnology*, Vol. 2. (Nalwa H.S., Ed.) Valencia, California, USA: Am. Sci. Publishers, **2004**, 565–585.
46. Lomova T.N., Andrianova L.G. *Zh. Neorg. Khim*. **1994**, *39*, 2011–2016.
47. Remy H. *Textbook of Inorganic Chemistry*, Vol. 1. (Geest & Portig K.-G., Ed.) Leipzig, Germany: Academic Publishing Society, **1960** [Remy H., *Lehrbuch der Anorganischen Chemie*, Band I, (Geest & Portig K.-G., Ed.) Leipzig, Deutschland: Akademische Verlagsgesellschaft, **1960**].
48. Korolev V.V., Korolev D.V., Lomova T.N., Mozhzhuhkina E.G., Zakharov A.G. *Russ. J. Phys. Chem. A* **2012**, *86*, 504–508. DOI: 10.1134/S0036024412030181.
49. Huang S., Dong Z., Mu W., Strom V., Chai G., Varga L.K., Eriksson O., Vitos L. *Appl. Phys. Lett*. **2021**, *119*, 141909. DOI: 10.1063/5.0065067.

Received 16.05.2023
Accepted 12.10.2023